Calibrated absolute seafloor pressure measurements for geodesy in Cascadia

Matthew J. Cook[1], Erik K. Fredrickson[2], Emily C. Roland[3], Glenn S. Sasagawa[1], David A. Schmidt[4], William S. D. Wilcock[2], and Mark A. Zumberge[1]
[1]University of California San Diego, Scripps Institution of Oceanography
[2]University of Washington, School of Oceanography
[3]Western Washington University, College of Science and Engineering
[4]University of Washington, Department of Earth and Space Sciences

Corresponding author: Matthew J. Cook (m4cook@ucsd.edu)

Key Points:

- Campaign-style surveys of in situ, absolute calibrated ocean pressure measurements were made in the Cascadia subduction zone.
- These sensor-independent measurements act as long-term, absolute reference values that can be used in future vertical deformation studies.
- We document the sources of error in the technique and quantify the formal uncertainties of data collected from 2014 to 2017.

Abstract

The boundary between the overriding and subducting plates is locked along some portions of the Cascadia subduction zone. The extent and location of locking affects the potential size and frequency of great earthquakes in the region. Because much of the boundary is offshore, measurements on land are incapable of completely defining a locked zone in the up-dip region. Deformation models indicate that a record of seafloor height changes on the accretionary prism can reveal the extent of locking. To detect such changes, we have initiated a series of calibrated pressure measurements using an absolute self-calibrating pressure recorder (ASCPR). A piston-gauge calibrator under careful metrological considerations produces an absolutely known reference pressure to correct seafloor pressure observations to an absolute value. We report an accuracy of about 25 ppm of the water depth, or 0.02 kPa (0.2 cm equivalent) at 100 m to 0.8 kPa (8 cm equivalent) at 3,000 m. These campaign survey-style absolute pressure measurements on seven offshore benchmarks in a line extending 100 km westward from Newport, Oregon from 2014 to 2017 establish a long-term, sensor-independent time series that can, over decades, reveal the extent of vertical deformation and thus the extent of plate locking and place initial limits on rates of subsidence or uplift. Continued surveys spanning years could serve as calibration values for co-located or nearby continuous pressure records and provide useful information on possible crustal deformation rates, while epoch measurements spanning decades would provide further limits and additional insights on deformation.

Plain Language Summary

The Cascadia subduction zone has produced large earthquakes and tsunamis whose potential size and interval is affected by the amount and distribution of locking between the tectonic plates. A large portion of the subduction zone is offshore, where typical land- and satellite-based methods are ineffective at measuring crustal deformation. Seafloor water pressure observations can be used to monitor height changes, but pressure gauges inherently drift at rates typically exceeding expected vertical seafloor deformation rates. The absolute self-calibrating pressure recorder

(ASCPR) measures the true, absolute, sensor-independent seafloor pressure by addressing and correcting sources of error caused by the internal piston gauge calibrator and recording pressure gauges. The accuracy of our measurements is about 25 ppm of the water depth, equivalent to 2.5 cm of height per 1,000 m of water. Campaign survey-style measurements using the ASCPR at seven benchmarks off the coast of Newport, Oregon from 2014 to 2017 establish a long-term record of absolute measurements that can be referenced by studies decades or more in the future or can be used to estimate and correct drift of nearby continuous pressure gauges. Continued measurements can provide more valuable information and insights on seafloor deformation and thus locking in Cascadia.

1 Introduction

The Cascadia subduction zone poses considerable seismic and tsunami hazard to the coasts of northwestern USA and southwestern Canada, stretching 1,300 km from Mendocino, CA to Vancouver Island, BC (Walton et al., 2021). Large tsunamigenic earthquakes have ruptured along the subduction zone numerous times in the past based on records of tsunami inundation, turbidite flows, and paleoseismic evidence, most recently in 1700 (Atwater et al., 2005). The recurrence interval of large earthquakes and tsunamis is suggested to be a few hundred years to a thousand years; the current state of the subduction zone is not well-known (Atwater, 1987). More information regarding the structure, deformation, and other properties of the subduction zone is needed to better characterize the seismic and tsunami hazards in Cascadia. Although land-based studies investigating interseismic and slow slip phenomena in Cascadia have been increasingly common over the last decades, terrestrial data alone are insufficient for constraining properties in the up-dip portion located offshore (Wang & Trehu, 2016).

Marine geodetic methods have been demonstrated over the last several decades. Acoustic methods, notably GNSS-Acoustic, can measure horizontal motions at the cm-level, and have been used to make measurements in various subduction zones, including Japan and Cascadia (Spiess et al., 1998; Matsumoto et al., 2008). Seafloor pressure, a proxy for seafloor height, is also widely used to measure vertical crustal motion and deformation. To be useful for seafloor geodesy, pressure variations caused by oceanic and atmospheric variations must be extracted from the seafloor pressure measurements to reveal the tectonic signal of interest. Although standard pressure gauges are capable of mm-level resolution, they are unreliable for measurements over months-to-years due to inherent drift (Polster et al., 2009). Pressure gauge drift contaminates and often exceeds long-term signals of interest and is difficult to reliably characterize. Methods to correct sensor drift include mobile pressure recorder (MPR) surveys by ROV, which measure pressure changes relative to a stable reference site (e.g., Stenvold et al., 2006; Chadwick et al., 2006; Nooner & Chadwick, 2009; Nooner & Chadwick, 2016), mobile pressure calibrator surveys by ROV, which provide a controlled, calibrated pressure reference adjacent to long-term in situ pressure recorders (Machida et al., 2020), normal self-calibrating pressure recorders (SCPRs), which measure pressure changes relative to a piston-gauge calibrator (Sasagawa & Zumberge, 2013; Sasagawa et al., 2016), and A0A (also known as AZA) sensors, which measure pressure changes relative to the internal air pressure (Wilcock et al., 2021).

The standard SCPR addresses gauge drift in situ by using a mechanical piston-gauge calibrator (PGC) to intermittently produce a stable reference pressure close to the ambient seafloor pressure. Drift in continuously recorded pressure gauges that are switched by a valve between the ambient ocean pressure and the PGC reference pressure can then be accurately

93 determined, and the drift can be corrected. In this mode of operation, the actual value of the PGC
94 reference need not be known accurately, we only require that it remains stable for the duration of
95 its deployment, i.e., unknown but constant offsets are acceptable (Sasagawa & Zumberge, 2013;
96 Sasagawa et al., 2016).
97 An alternative use of the standard SCPR technology is to accurately account for every
98 measurement parameter in an absolute manner that is traceable to metrological standards and
99 then periodically deploy in a campaign style rather than continuously occupying one location. In
100 this fashion, a single instrument can be used to survey several locations. Because the absolute
101 value of the pressure on top of a benchmark is determined at each visit, we call this method the
102 Absolute Self Calibrating Pressure Recorder, or ASCPR. The instrument is carried and handled
103 by ROV, placed on a permanent seafloor benchmark (a concrete disc or similar platform), and
104 alternately records the ocean and the reference pressures for several hours. Knowledge of the
105 reference pressure's true value enables the absolute pressure on the benchmark to be determined.
106 The permanent benchmarks facilitate accurate re-positioning of instruments for all observations.
107 Since the pressures measured by the ASCPR are determined absolutely, each survey contributes
108 to a time series of point measurements and any future observations can be compared to earlier
109 ones even if different components or a different absolute sensor are used.
110 The absolute seafloor pressure measurements must be addressed within the context of the
111 overlying water column and atmosphere to isolate the tectonic signal. The ocean tides are aliased
112 in our records but can also be accounted for within a few cm through tidal predictions or models
113 (Agnew, 2012; Pawlowicz et al., 2012). Ocean variability at periods longer than the tides can be
114 aliased in each survey and present additional challenges. Averaging over many years can
115 ameliorate that problem, though a refinement to the method is to leave a continuously recording
116 bottom pressure recorder (BPR) at each benchmark to capture and account for seafloor pressure
117 variations attributed to these processes. Further improvements can be made by addressing these
118 processes using available regional pressure networks, satellite altimetry products, and CTD data
119 (Frederickson et al., 2019; Watts et al., 2021).
120 We conducted pressure surveys with an ASCPR along a trench-perpendicular profile in
121 the Cascadia subduction zone over a four-year period from September 2014 to September 2017.
122 We present the design and methods of the instrument and surveys, as well as absolute seafloor
123 pressure values, which will serve as longstanding fiducial values for future studies and estimated
124 secular rates. We also document the sources of error and report on the repeatability of the
125 technique.
126
127 **2 Method**
128 The ASCPR instrument consists of a 40 cm diameter spherical pressure case that houses a
129 PGC (which generates a pressure by applying a mass force over a piston area), the mechanical
130 components needed to constrain the PGC mass during transit and deployment and spin the mass
131 during measurements, gimbals to level the PGC, two redundant quartz pressure gauges, and
132 valves to pressurize the PGC and alternately switch the gauges between the ambient seafloor and
133 reference pressures. The mass lock system prevents unwanted and potentially harmful torque on
134 the PGC system during transit. The mass spin-up system allows the PGC to generate a smooth,
135 continuous reference pressure and avoid pressure spikes caused by stick-slip behavior. The
136 spherical pressure case is mounted in a three-legged aluminum frame suitable for handling by an
137 ROV. Before each deployment a mass is loaded internally onto the system's piston of appropriate
138 size to create a reference pressure slightly less than the local seafloor pressure. This allows the

hydraulic connection to ambient sea pressure to pressurize the PGC, obviating the need for a high-pressure pump, and minimizes the likelihood and amount of detectable hysteresis. In the survey reported on here, the mass was transferred in the vessel's freezer held at seafloor temperature and the instrument was kept there during transits between sites to help minimize thermal effects during the measurement.

The ASCPR is turned on while connected to the ROV on the ship deck and starts recording pressure data, ancillary measurement data, and state-of-health data at 1 Hz. The ROV carries the ACPR to depth in the basket. Once on site, the ROV places the ASCPR on top of a pre-deployed seafloor benchmark and remains in place, electrically connected to the instrument, for the duration of the measurement. An operator on the vessel sends commands to the system to actuate internal gimbals to level the PGC, unlock the mass, pressurize the PGC, engage the rotation mechanism to spin the mass (this ensures the PGC is in a state of kinetic friction to minimize pressure spikes caused by stick-slip behavior), and control the valve which alternates the quartz gauges between sea pressure and PGC pressure. Gauge drift and errors are present in the gauge output, whether the gauge is observing the reference pressure or ambient seafloor pressure. Alternating the gauge output between the PGC reference pressure and ambient seafloor pressure allows us to apply corrections determined from the reference pressures to the seafloor pressures. Ambient sea pressure is buffered by a tube containing sebacate oil to prevent seawater from entering the PGC. A typical measurement period spans about two hours, with five to seven cycles alternating between 10- to 15-minute-long seafloor and reference pressure observations.

2.1 Survey profile

The calibrated pressure surveys were conducted on seven concrete benchmarks at six sites that form a trench-perpendicular profile off the coast of Oregon at 44.5° N (Figure 1, Table 1). The farthest west station (O1) is located 105 km offshore on the Juan de Fuca Plate side of the trench at 2900 m water depth. The other stations (O2, O2B, O3, O4, O5, and O6) are located on the North American plate and are separated by approximately 15 km from each other towards shore. The closest station to shore (O6) is about 20 km off the coastline at a depth of 70 m. Each station had an autonomous, continuous BPR attached to the benchmark or located nearby. A redundant benchmark (O2B) was established adjacent to O2 when a second set of BPRs was deployed.

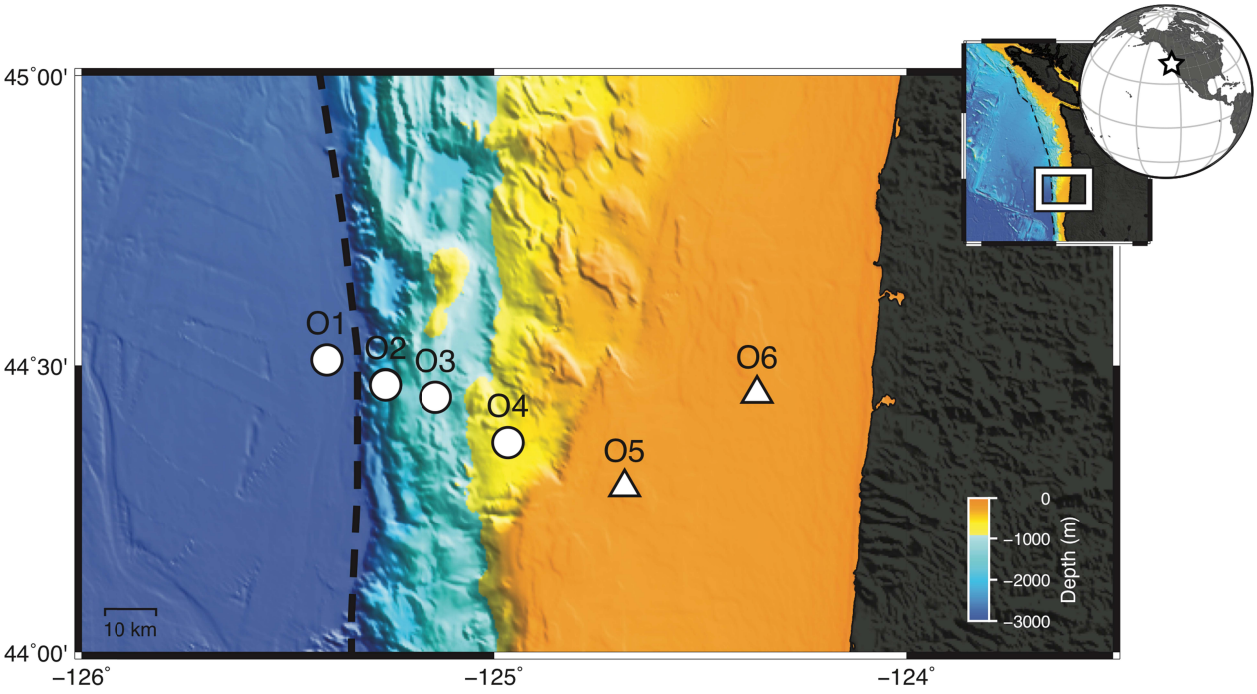

Figure 1. Map of the survey area in the Cascadia subduction zone. The black dashed line indicates the deformation front at the foot of the accretionary prism. Circles represent standard benchmarks and triangles represent trawl-resistant benchmarks.

Two types of solid concrete benchmarks were used depending on the water depth, expected seafloor material, and nearby trawling activity. The benchmarks located in deeper water (O1, O2, O2B, O3, and O4) are based on a design originally developed by Segawa and Fujimoto (1988) and later used in a variety of deep ocean settings (e.g., Chadwell, 2016). They have circular bases 76.2 cm in diameter, 15 cm thick, with three 14 cm long legs protruding below, weighing a total of 66.7 kg in water (145 kg in air). The shallow water benchmarks (O5 and O6) are a trawl-resistant design with a triangular base that slopes up to a platform 71.1 cm across and weigh 354 kg in water (770 kg in air). Figure 2 includes photographs of each type of benchmark on the seafloor.

The benchmarks were coarsely leveled using the ROV manipulator to nudge them in a particular direction to within a few degrees of level. The total tilt of the benchmark is inconsequential if it is less than 10°, which is the amount of tilt the ASCPR gimbals can accommodate. The tilt at each benchmark was measured using the internal tiltmeter and recorded as a reference for future occupations to monitor the stability or potentially identify gross disturbances of the benchmarks (Table 1).

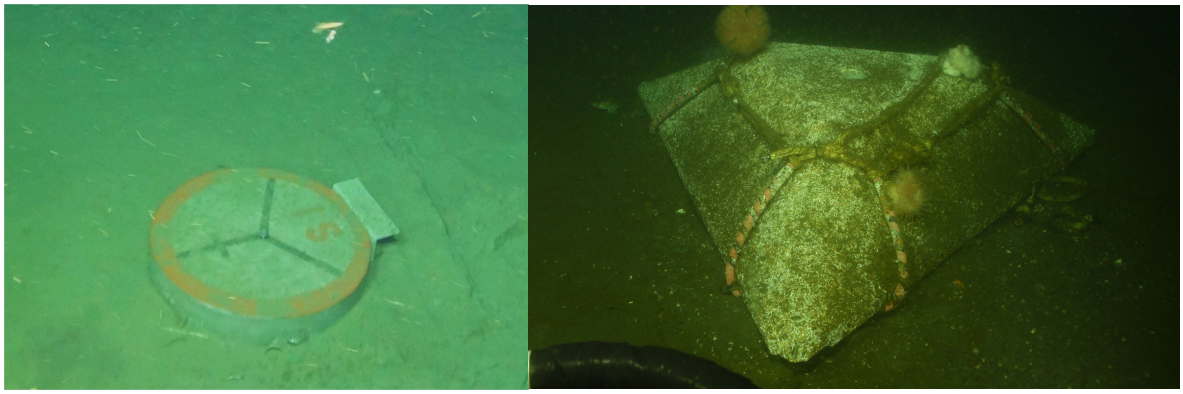

Figure 2. Photographs of benchmarks. The left shows a standard circular benchmark at O1, a deep site (depth greater than ~400 m), and the right shows a trawl-resistant benchmark at O5, a shallow site (depth shallower than ~400m or located near known trawl zones).

Table 1. Basic station information. Benchmark tilts are listed as a reference for future occupations. Uncertainties are the quadrature sum of the tiltmeter accuracy and standard deviation of measurements conducted each occupation.

Station	Latitude (°N)	Longitude (°E)	Depth (m)	Benchmark tilt (°)	Established (year)
O1	44.5099	-125.4056	2907	4.0 ± 0.2	2014
O2	44.4670	-125.2636	1909	0.5 ± 0.1	2014
O2B	44.4661	-125.2637	1910	0.9 ± 0.1	2015
O3	44.4450	-125.1418	1315	3.4 ± 0.1	2016
O4	44.3666	-124.9670	620	0.3 ± 0.1	2016
O5	44.2889	-124.6838	79	3.4 ± 0.2	2016
O6	44.4512	-124.3616	70	3.0 ± 0.1	2016

2.2 Absolute determination of the PGC reference pressure

The ASCPR method relies on accurate determinations of the true, absolute value of the PGC reference pressure. The quartz-gauge observations of the PGC reference pressure reveal static offsets from imperfect calibrations and transients from thermal gradients, creep, or other unmodeled effects in the quartz gauges (Wearn & Larson, 1982; Polster et al., 2009). These offset and transient errors are present in the gauge output regardless of the gauges being directed to the reference pressure or ambient seafloor pressure. These errors are determined using the pressure difference between the actual, absolute, known PGC reference pressures and the observed gauge output during calibration intervals. Alternating the gauges between the PGC and ambient seafloor pressure allows us to apply the absolute gauge corrections to the seafloor pressure record as well. We do not expect any detectable hysteresis since our target reference pressure is chosen to be within about 200 kPa of the expected seafloor pressure. As a result, the seafloor pressure values are calibrated and traceable to absolute standards.

Equation 1 and Table 2 define the PGC reference pressure, P_{PGC}, and the significant variables (Bean, 1994). We measure and determine the absolute values and uncertainties of each correction term using NIST-traceable standards either prior to or during a deployment.

$$P_{PGC} = \frac{M\left(1 - \frac{\rho_{air}}{\rho_{mass}}\right) g\left(1 - \frac{\theta^2}{2}\right) + \gamma C}{A(1 + bP_0)[1 + 2\alpha(T - T_0)]} + P_{baro} \#(1)$$

Table 2. Reference pressure variables and notes about their values and how they are determined or measured.

Variable	Term	Comments
P_{PGC}	Pressure, PGC (kPa)	Piston gauge calibrator
M	Mass (kg)	Measured in lab (2016)
g	Gravitational acceleration (m/s^2)	Götze 2011 gravity formula + EGM2008 gravity anomaly + seawater gravity gradient
A	Piston area (m^2)	Fluke (2014)
θ	Tilt (rad)	Measured by Jewell 900 sensor; calibration of conversion coefficients done in lab (2014)
ρ_{air}	Internal air density (kg/m^3)	Calculated using ideal gas law for N_2, P_{baro}
ρ_{mass}	Mass density (kg/m^3)	Calculated using mass materials information
γ	Viscosity (m^2/s)	Nominal value of sebacate oil
C	Piston circumference (m)	Calculated from area value; Fluke (2014)
b	Coefficient of elastic deformation (1/Pa)	Fluke (2014)
P_0	Fluid pressure (Pa)	Calculated using simplified reference pressure ($P = Mg/A + P_{baro}$)
α	Linear coefficient of thermal expansion (1/°C)	Lab calibration (2018)
T_0	Reference temperature (°C)	Nominal value from DHI Fluke
T	Piston temperature (°C)	Measured by Fluke PRT; calibration of conversion coefficients done in lab (2016)
P_{baro}	Internal air pressure (Pa)	Measured by Vaisala PTB 110; conversion coefficients lab calibration (2016)

Table 3 provides the accuracy of each individual variable and the total measurement accuracy. Some of the terms in equation (1), such as temperature and internal air pressure, change on timescales shorter than the duration of a calibration, and are measured in situ.

In shallow waters, typically 100 m to a few hundred m deep, the primary error constituents are the internal air pressure and then the piston-cylinder cross-sectional area. The internal air pressure has an accuracy of 0.02 kPa within the nominal range and our operating range, corresponding to up to 20 ppm (at 100 m water depth). The piston-cylinder cross-sectional area for the larger diameter apparatus used for smaller pressures and shallower water depths has

a manufacturer provided accuracy of 14 ppm, which corresponds to about 0.01 kPa at 100 m water depth, or 0.1 kPa at 1,000 m water depth. Other errors are small on the order of a few ppm and contribute a small fraction of the total error.

At greater depths of several hundred m to several km, the error is dominated by the piston-cylinder area. The internal air pressure accuracy remains 0.02 kPa but constitutes a significantly smaller error contribution of 2 ppm (at 1,000 m depth) or less. The piston-cylinder used for greater depths and pressures is a smaller diameter and has a lower cross-sectional area accuracy of about 25 ppm. As the water depth and reference pressure increase, the error also increases, reaching nearly 0.8 kPa at 3,000 m. The greatest improvement to our deep water measurements would be improving the accuracy of the piston-cylinder area, but that requires micrometer-level measurements of the piston-cylinder dimensions. Facilities equipped to do this are rare and prohibitively expensive. The error is otherwise the same as the shallow depths, where most of the remaining errors are small and contribute little to the total error.

Table 3. Uncertainties of each reference pressure variable (or collective term) and the total quadrature sum error of a resulting calibration measurement. Some uncertainties scale with pressure (depth) while others do not. Three example depths are provided to highlight the uncertainty magnitude at various pressures (depths). A 10 ppm uncertainty at 1,000 m depth corresponds to 1 cm in height.

Name	**Variable**	**Accuracy**	**Example depth**		
			100 m	**1,000 m**	**3,000 m**
Mass	M	(Minimum 14.648 kg) 0.9 ppm (Maximum 3.029 kg) 4.3 ppm	3.7 ppm	4.3 ppm	0.9 ppm
Gravitational acceleration	g	2.3 ppm	2.3 ppm	2.3 ppm	2.3 ppm
Piston area	A	(PC-7300-200) 14 ppm (PC-7300-2) 25 ppm	14 ppm	25 ppm	25 ppm
Thermal expansion	$[1+2\alpha(T - T_0)]$	4.1 ppm	4.1 ppm	4.1 ppm	4.1 ppm
Buoyancy	$\left(1 - \frac{\rho_{air}}{\rho_{mass}}\right)$	(Stainless Steel Mass) 1.5 ppm (Aluminum Mass) 3.3 ppm	3.3 ppm	1.5 ppm	1.5 ppm
Tilt	$\left(1 - \frac{\theta^2}{2}\right)$	1.6 ppm	1.6 ppm	1.6 ppm	1.6 ppm
Elastic deformation	$(1+bP_0)$	(PC-7300-200) 1.1 ppm (PC-7300-2) 0.03 ppm	1.1 ppm	0.1 ppm	0.03 ppm
Surface	χC	(PC-7300-200)	2 ppm	0.5 ppm	0.17 ppm

tension		0.002 kPa (PC-7300-2) 0.005 kPa			
Internal air pressure	P_{baro}	0.02 kPa	20 ppm	2.0 ppm	0.67 ppm
Quadrature Sum Total	—	—	**25.5 ppm**	**26.0 ppm**	**25.6 ppm**

The values used to determine the reference pressure at each station and typical ranges for measured variables are provided in Table 4, while the exact values can be found in the ancillary data. For example, the barometric pressure within the sphere typically changes by 5-10 kPa during a calibration owing to the changing temperature inside the sphere. The internal temperature increases because of the electronics inside that are turned on when a survey is initiated, and a measurement sequence begins.

Table 4. Values used to determine the known reference pressure at each station. Tilt, piston-gauge temperature, and internal air pressure are measured in situ. Their values vary between each occupation and can fall within a broad, nominal range that is listed; however, they typically fall within a narrower range that is also specified. Their exact values can be found in the ancillary data records.

Variable	**Value at Station**				
	O1	**O2 / O2B**	**O3**	**O4**	**O5 / O6**
M (kg)	14.648207	9.539057	6.544407	3.029427	3.509207
g (m/s^2)	9.80496	9.80522	9.80540	9.80553	9.80555
A (10^{-6} m^2)	4.901758				49.02159
θ (10^{-3} rad)	Ranges from (-1.7, 1.7) but typically within (-0.87, 0.87)				
ρ_{air} (kg/m^3)	Ranges from (0.71, 1.03) but typically within (0.81, 0.95)				
ρ_{mass} (kg/m^3)	7779.907	5586.182	7613.153	3324.631	3230.054
γ (m^2/s)	0.031				
C (10^{-3} m)	7.84839				24.8198
b (10^{-13} 1/Pa)	7.54				12.6
P_0 (kPa)	29,372 +/- 10	19,153 +/- 10	13,163 +/- 10	6,132 +/- 10	774 +/- 10
α (10^{-6} 1/ °C)	3.9				
T_0 (°C)	20				
T (°C)	Ranges from (4.5, 9.5) but typically within (5, 8.5)				
P_{baro} (kPa)	Ranges from (60, 85) but typically within (67.5, 77.5)				

The pressure observed by the gauges while valved to the ambient seawater is denoted P_{sea}^{obs} and contains the tectonic vertical deformation signal of interest, as well as any variation in the overlying water column. The pressure observed while valved to the PGC is denoted P_{PGC}^{obs}. Each differs from their absolute counterparts, P_{PGC} and P_{sea} respectively, by the same error, P_{error}, attributed to imperfections mentioned above.

$$P_{PGC}^{obs} = P_{PGC} + P_{error} \#(2)$$

$$P_{sea}^{obs} = P_{sea} + P_{error} \#(3)$$

The gauge error, P_{error}, is equal to the difference between the observed calibration pressure and the true calibration pressure.

$$P_{error} = P_{PGC}^{obs} - P_{PGC} \#(4)$$

We chose to model P_{error} as a constant offset and a relatively small, time varying component modelled with combined exponential and linear terms (Wearn & Larson, 1982; Watts & Kontoyiannis, 1990; Polster et al., 2009). Other numerical drift models exist, but the exponential component of a few cm sufficiently captures any short-term transients caused by viscoelastic creep or thermal effects, and the long-term linear component represents any long-term mechanical creep, outgassing, or aging of the quartz crystal (Paros & Kobayashi, 2015a). The exponential component is modeled starting at the initial time, t_0, of the first calibration interval for an occupation and extending until the last time of the final calibration interval, with an amplitude, A, and time constant, B, typically on the order of a few minutes. The linear rate, C, is also modeled relative to the initial time, t_0, and the offset is simply determined as D.

$$P_{error} = Ae^{-\frac{t-t_0}{B}} - C(t - t_0) + D \#(5)$$

A non-linear least squares regression is used to calculate the best-fit coefficients and drift model to the gauge error time series defined as the difference between P_{PGC} and P_{PGC}^{obs}. The true sea pressure is computed by correcting P_{sea}^{obs} with the modeled error function, which is the same whether the valve connects the gauges to the PGC or the ambient ocean.

2.3 Absolute pressure occupation

Pressure time series show fluctuations related to the descent of the ASCPR to the seafloor and the flipping of the value between ambient and reference pressures (Figure 3). In (a), the pressure observed by one of the two redundant gauges over the course of a survey is plotted in grey (before and after a calibration) and black (during a calibration). The grey trace reveals that the instrument was taken to depth by the ROV just before 21 October 2015 at 00:00 and placed on the benchmark around 04:45 where, being stationary, it began to show the tidal pressure variation. The dotted green trace shows the predicted ocean tides. Soon after being emplaced on the benchmark, the gauges were alternately valved between the ambient seawater and the PGC reference pressure, the latter being around 200 kPa less than the sea pressure at this site. This creates an approximate square wave in pressure that covered seven valve cycles each lasting about 20 minutes. In (b), the raw observations of the two quartz gauges, P_{PGC}^{obs}, are plotted in red shades during the times they were valved to the PGC reference. The known output of the PGC (equation 1) as a function of time, P_{PGC}, is plotted in black at the same times (labeled "Known Reference" pressure). One can see that P_{error} is primarily an offset of about 12 kPa for gauge #1 and 9 kPa for gauge #2. The time variations in both the gauge records and the known PGC record are too small to be visibly discerned in this plot. In (c), the records from the two uncalibrated gauges are plotted during the periods when the valve connected them to the outside seawater, P_{sea}^{obs}; the tidal signal is apparent. The offset between the two further exemplifies their imperfect calibrations, P_{error}. In (d), two P_{error} functions, determined independently for each

316 gauge from the records shown in (b), have been added to the two corresponding records plotted
317 in (c), yielding the final, absolutely calibrated seafloor pressure records, P_{sea}. The traces from the
318 two gauges lie on top of each other, as they should confirming the agreement of the corrections.
319 In (e), the small differences between the two gauges are plotted partly confirming the efficacy of
320 the method. A perfect calibration method for two independent gauges sensing the same pressure
321 source should entirely remove any differences between the two records. The difference between
322 the two calibrated pressure gauges is practically flat at zero, although small coherent variations
323 (apparent as stripes or steps) persist. These are likely due to noise in the applied calibrations and
324 a very small timing offset between the two gauges but are inconsequential and treated as noise.
325

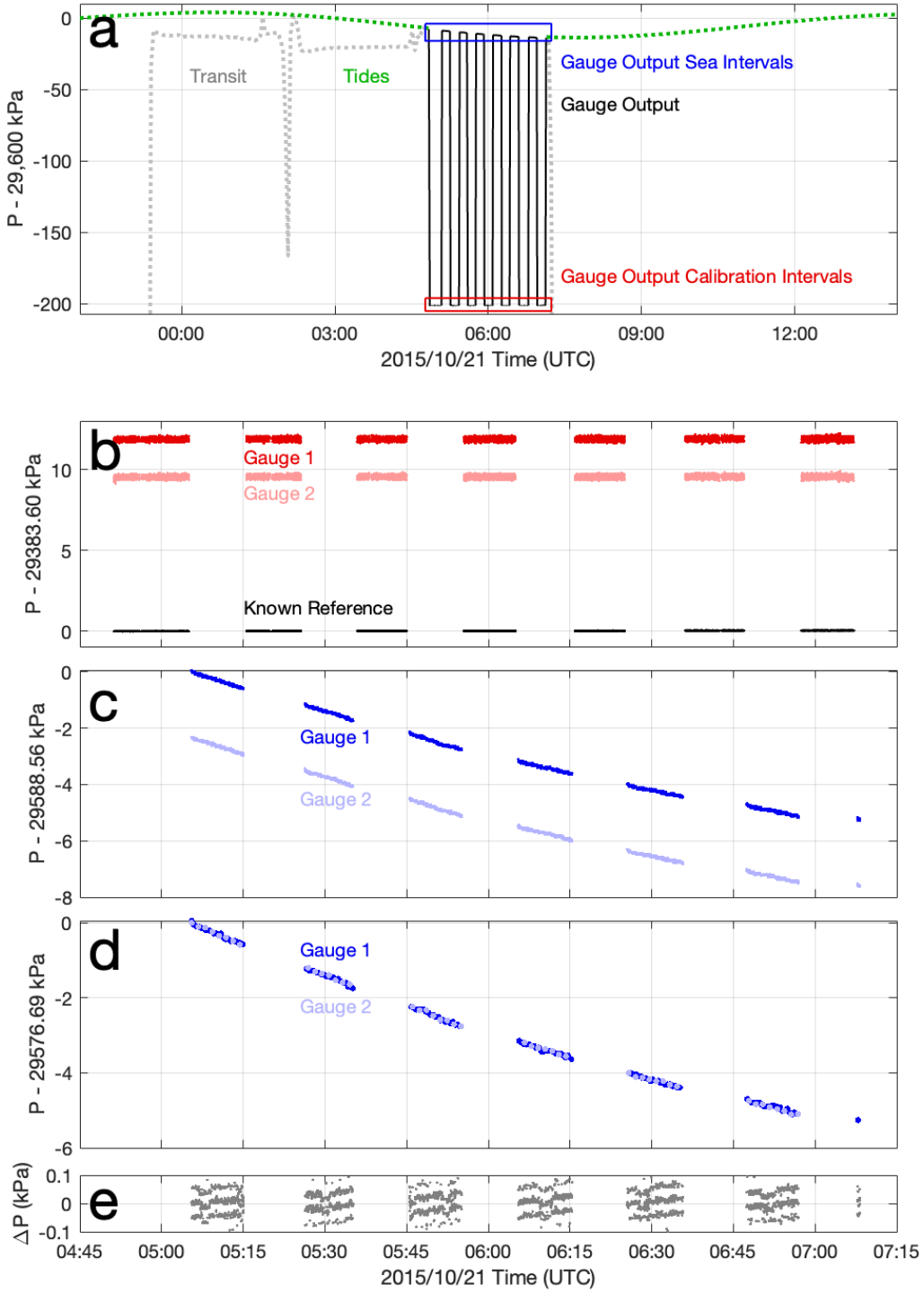

Figure 3. Pressure records during a typical ASCPR measurement at station O1 in 2015. (a) Raw pressure gauge output before (dashed grey line), during (solid black line), and after (dashed grey line) occupying the station for a measurement. Predicted ocean tides for the station are shown (dashed green line). The gauge output during calibration intervals is in the red box, shown in greater detail in (b). The gauge output during ambient seafloor pressure intervals is in the blue box, shown in greater detail in (c). (b) Observed output of the two gauges during calibration intervals (dark and light red) and the calculated time series of the known reference pressure

defined in equation (1). The raw gauge output is different from the known reference by an offset and exponential-linear drift function. (c) Observed output of the two gauges during ambient seafloor intervals (dark and light blue). The raw gauge output is also different from the true, absolute seafloor pressure by the same offset and exponential-linear function determined from (b). (d) Absolutely calibrated seafloor pressures at the height of the bottom of the piston-gauge. (e) The difference between the two calibrated pressure records (dark and light blue traces in (d)) as an indication of the method efficacy. The difference is nearly flat and centered at zero, meaning the independent corrections applied to each gauge effectively capture each gauge drift signal and produce no differential signal. Coherent noise is still present, mostly attributed to noise in ancillary data used in the corrections.

2.4 Height correction

As a final correction, the pressure values measured by the ASCPR must be transferred to the height of the surface of the concrete benchmark, 32.6 cm below the height of the piston-gauge (Figure 4). The in situ calibration of the quartz pressure gauges as described above establishes a function, P_{error}, that, when added to the raw gauge outputs, gives values equaling the known pressure at the height of the piston-gauge. While the quartz gauges are physically separated from the piston-gauge and therefore experience a pressure difference from the associated pressure head, this offset is included in P_{error} – that is, the corrections to the quartz gauges incorporate both the gauge imperfections and the pressure head relative to the bottom of the piston-gauge. There is a hydraulic line filled with sebacate oil in the internal system that emerges in seawater through a port 12.1 cm below the bottom of the piston, and this port is 20.5 cm above the benchmark. The pressure head correction from the calibrated pressure measurement and the benchmark is therefore:

$$\Delta P = \rho_S g \times 0.121 \text{ m} + \rho_W g \times 0.205 \text{ m}$$

where ρ_s and ρ_w are the densities of sebacate and seawater respectively, and g is the value of gravity. Values for ρ_s and ρ_w are slightly site dependent because they depend on ambient pressure. For ρ_S we use equation (2) from Paredes et al. (2012) assuming a temperature of 5 ºC and standard estimates for ρ_W. Table 5 lists the necessary terms and resultant height corrections for our sites.

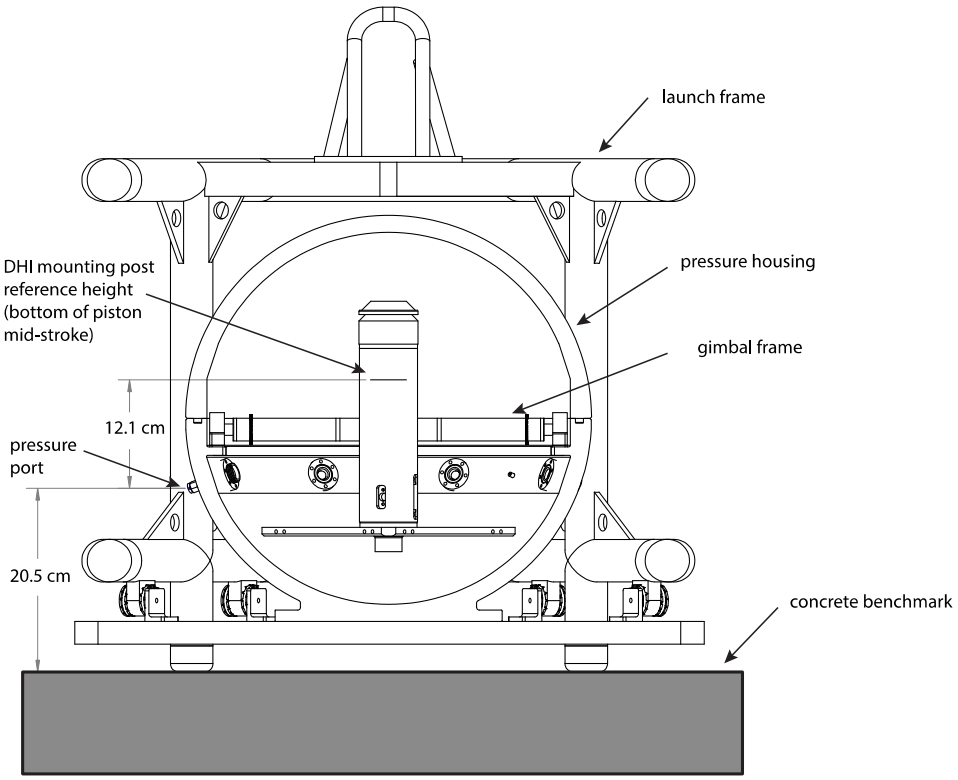

Figure 4. A cross-sectional drawing of the instrument in its spherical housing and frame. The height of the bottom of the piston-gauge is where the reference PGC pressure is determined. A correction to the benchmark 32.6 cm below depends on the fluid density in between, which is oil for part of the path and water for another portion. Note that the height of the piston bottom above the benchmark center varies only by an inconsequential amount in cases where the benchmark is not level.

Table 5. Terms used to determine the height correction for transferring absolute pressure measurements from the piston inside the ASCPR to the surface of the benchmark.

Station	Depth (m)	ρ_s (kg/m^3)	ρ_w (kg/m^3)	Gravity (m/s^2)	Height correction (kPa)
O1	2907	940	1041	9.80496	3.21
O2	1909	934	1036	9.80522	3.19
O2B	1910	934	1036	9.80522	3.19
O3	1315	931	1033	9.80540	3.18
O4	620	927	1030	9.80533	3.17
O5	79	925	1025	9.80555	3.16
O6	70	925	1025	9.80555	3.16

2.5 Continuous pressure recorders

After removal of the ocean tides, physical oceanographic processes cause seafloor pressure fluctuations that can eclipse tectonic signals of interest such as secular strain accumulation or slow slip events (Frederickson et al., 2019; Watts et al., 2021). These processes include internal waves, currents, eddies, El Niño Southern Oscillation (ENSO), and other decadal-scale events, which can contribute 5 cm or more of noise at periods from hours to years (NRC 2012). When we infer the seafloor height from the absolute pressure campaigns, we have aliased many of these oceanographic processes. Some methods to reduce the oceanographic variability and noise include using surrounding pressure data, specifically at a comparable depth, or satellite altimetry and CTD data (Frederickson et al., 2019; Watts et al., 2021).

Co-located or nearby continuous pressure data can provide direct and valuable information on the oceanographic signals that are otherwise aliased in our surveys. Over time spans shorter than a couple decades, these data can provide significant improvements through direct observations of oceanographic processes. Even though these signals tend to average out in long time series spanning several decades, the data can still contextualize individual surveys. Additionally, since ASCPR measurements produce accurate absolute seafloor pressure values, the surveys can be used as calibration points to estimate and correct long-term linear drift in continuous gauges. After correcting for drift, the full-rate continuous time series can be processed to address oceanographic variability and used to estimate deformation rates. We deployed a continuous BPR at or near each site to provide high-rate data during and between surveys. All the BPRs used Paroscientific quartz pressure gauges but different sensor configurations were used to accommodate different depths, durations, and logistical needs.

One BPR from the Applied Physics Laboratory (APL) at the University of Washington (UW) was installed near station O1 on the OOI Cabled Array in September 2014. It housed a Paroscientific model 46K pressure gauge in a titanium housing. Data were recorded at 1-sec intervals and telemetered to shore in real-time to shore at the OOI Data Portal. An OOI Cabled Array BPR was also installed as part of a Benthic Experiment Package near station O4, but the sensor was changed, replaced, or out of service for most of the time spanning our surveys.

Two BPRs were constructed at the Scripps Institution of Oceanography (SIO) at the University of California, San Diego (UCSD). These were deployed at the 1900 m depth site, O2. They used battery powered Paroscientific model 46K pressure gauges inside aluminum pressure cases. Data were integrated over 100-sec intervals and recorded to an internal memory card. The data were recovered from the internal memory after the instruments were physically recovered.

Another five BPRs were built by the UW APL. Two were designed for shallow water less than 100 m depth (stations O5 and O6) and used Paroscientific model 2200A pressure gauges inside PVC pressure cases. The other three were designed for greater depths ranging from 600 m to 1900 m (stations O2, O3, and O4) and used Paroscientific model 31K, 42K, and 43K pressure gauges housed inside titanium pressure cases. They all recorded at 15-sec intervals to internal memory. Data were recovered wirelessly using a RF antenna linked to an ROV-held receiver a few cm away to prevent disturbing the instruments when possible. In other instances, data were recovered from internal memory after the instrument was recovered. These sensors were designed to record for up to 10 years from when they were deployed.

The four separate BPR deployments at stations O2 and O2B lasted between 8 and 15 months and overlapped with the previous BPR by at least a few days. Although these records could be concatenated to produce a single continuous record by matching the overlapping data intervals, we are unable to reliably distinguish drift in the former record from drift in the latter record. The linear drift rate could be estimated from data later in the record, but we have no way

to estimate the exponential drift, which is typically significant in the first 90 days, though longer exponential time constants have been observed (Polster et al., 2009). However, the records still provide observations and estimations of the oceanographic signals occurring during surveys but were not evaluated as a single, continuous record spanning all the surveys.

The BPRs at stations O3, O4, and O5 failed early on due to pressure housing leaks and we were unable to recover the continuous data for those sites. Therefore, continuous data at stations O3, O4, O5 are not included in this analysis since complete records were not available. The cause of the leaks was identified, and the instruments were modified and re-deployed. The BPR at O6 did not fully span both surveys and had timing offsets difficult to reconcile. Therefore, O6 is also not included in this analysis.

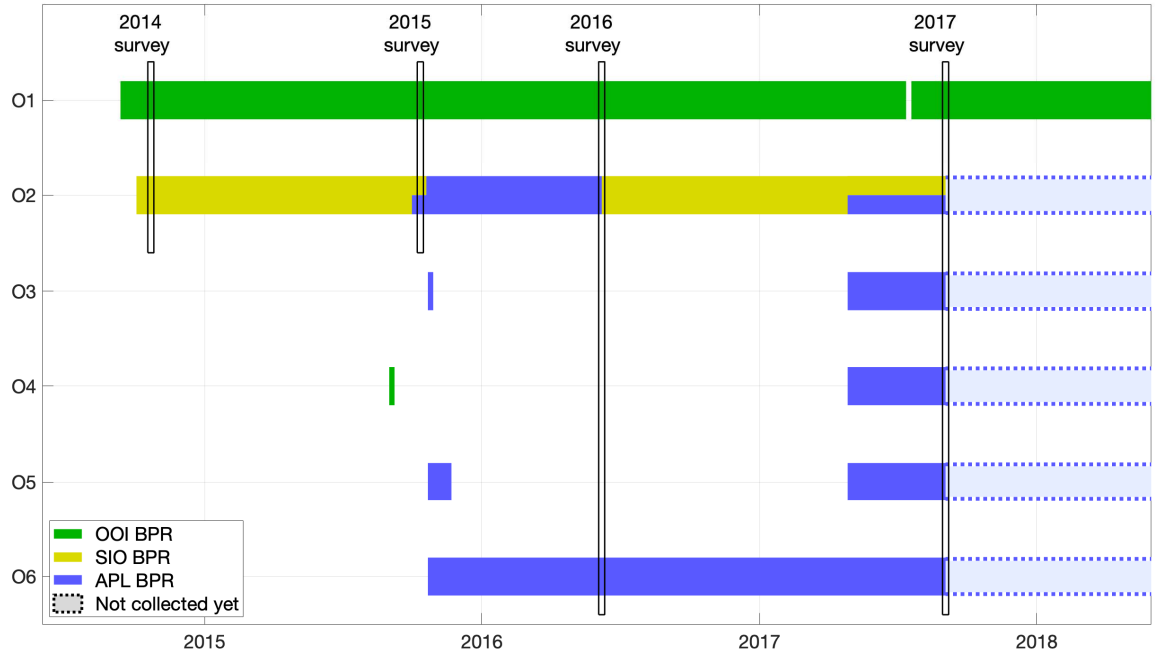

Figure 5. Timeline of continuous BPR data availability. ASCPR survey windows are boxed. Large gaps in the BPRs deployed at O3, O4, O5, and O6 are due to pressure housing leaks, which were identified, recovered, refurbished, and redeployed. The APL BPRs should be recording until about 2027 but data recovery requires an ROV or physical recovery. The OOI BPR has been recording continuously with only minor power interruptions.

2.6 Additional geodetic monumentation

Benchmarks placed on the seafloor acted as our primary measurement markers. In 2016, we deployed BPRs mounted to concrete seafloor benchmarks provided by APL near stations O2 and O2B, O3, O4, O5, and O6. These secondary BPR benchmarks included a platform wide enough to place our instruments. In 2017, we installed secondary geodetic monuments, which consisted of 4-m-long, 4.8-cm-diameter aluminum pipes jetted between 3 to 6 m deep into the seafloor sediment so that about 1 meter extended above the seafloor, at O1, O3, and O4. The pipe is better coupled to the sediment and provides a stable comparison monument within a few meters of the primary benchmark. The pipe was painted with alternating 15.0 cm long black and yellow stripes to increase visibility and provide a vertical length scale. A 15.3 cm by 40.3 cm

metal plate with yellow-painted edges was fastened to the top of the pipe with a firehose coupling to support a pressure recorder.

An MPR was used to make a total of four alternating, 5-minute-long seafloor pressure measurements between the primary benchmark and secondary benchmark: either a pole-mounted plate or secondary concrete benchmark. Secondary monuments will provide a means in future surveys to assess the stability of the primary benchmarks by repeating the MPR surveys between them. The MPR baseplate dimensions are close to the secondary monument top plates, so when the MPR is placed centered on the plate, the uncertainty attributed to variations in placement is very small. The pressure difference, a proxy for height difference, was calculated after a computed tide model using Some Programs for Ocean Tide Loading (SPOTL; Agnew, 2012) and combined exponential-linear drift were removed from the short survey. Table 6 lists the pressure differences between the surface of the primary concrete seafloor benchmarks and the heights of the plates on the secondary benchmarks. A height difference between the two can be determined using the local gravity and seawater density.

Table 6. Pressure differences between primary benchmarks and secondary geodetic monuments as measured by the MPR surveys. The difference is taken as the pressure at the primary benchmark minus the pressure at the secondary reference. Pressure uncertainties are single standard deviations.

Station	Secondary Reference	Pressure Difference (kPa)
O1	O1-pole	10.0 ± 0.1
O2	O2B	-6.6 ± 0.1
O2B	O2-APL benchmark	6.5 ± 0.1
O3	O3-pole	12.6 ± 0.1
O4	O4-pole	2.9 ± 0.1
O5	O5-APL benchmark	-20.5 ± 0.1

3 Results

We present the results in three forms. First, Figure 6 plots the corrected absolute sea pressures at the instrument reference height of the PGC for each occupation at each station. The pressures can be transferred to the benchmark surface by applying the appropriate height correction (Table 4). Table 7 provides the absolute seafloor pressure value recorded at the specified date and time and at the height of the piston-gauge calibrator, not including the height correction described in section 2.4 nor any tidal corrections corresponding to the plots in Figure 6. Once corrected for the instrument's height to the benchmark surface and an estimated tidal correction, these values form the basis for future decadal-scale absolute seafloor pressure measurements, which can be used to infer motions caused by tectonic deformation and changes in the overlying water column. These instrument-independent, fiducial measurements form the foundation for long-term surveys and studies of secular rates caused by tectonics and sea level rise.

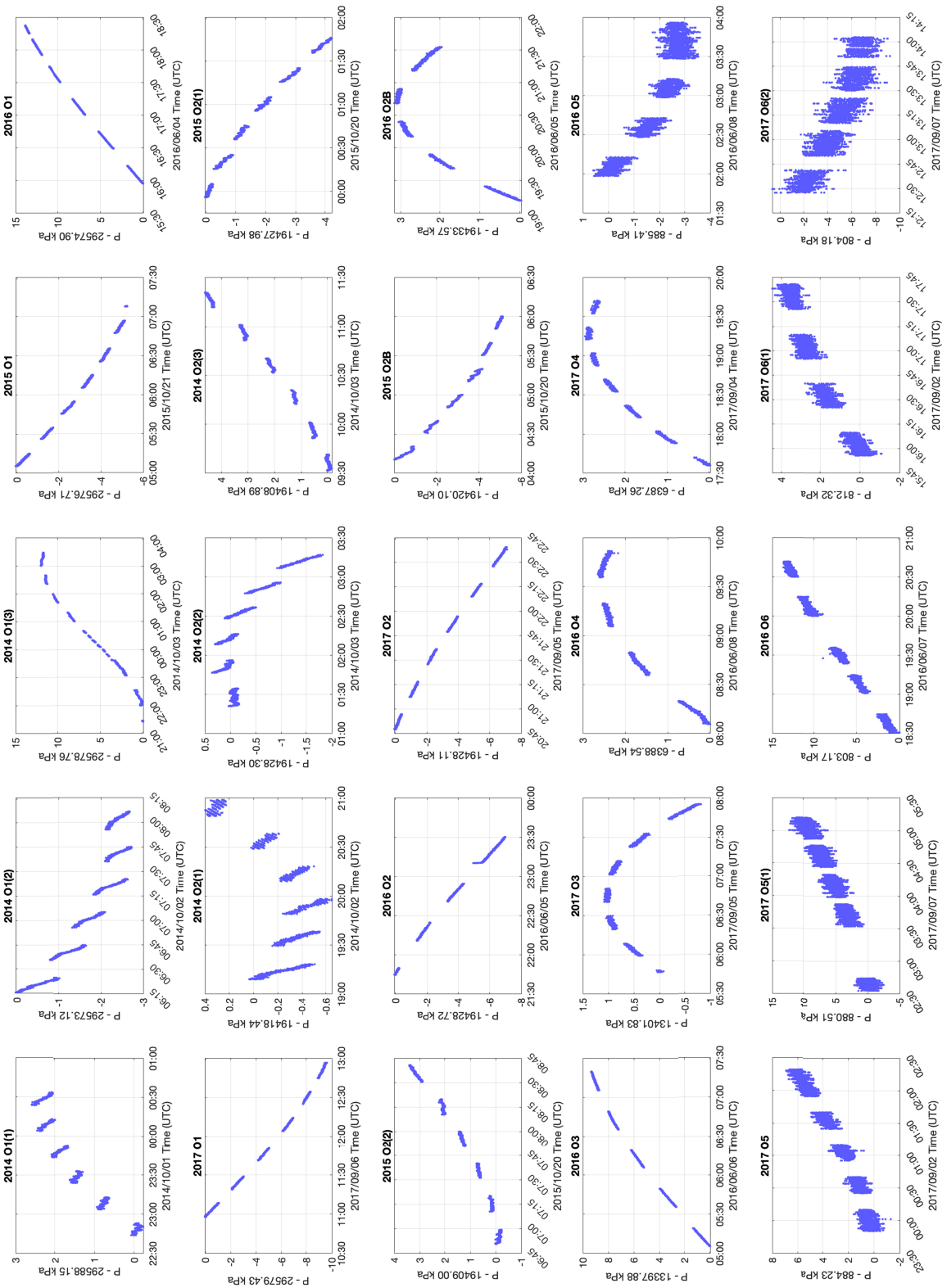

Figure 6. Corrected seafloor pressure records for each survey conducted at O1 through O6 between 2014 and 2017.

494 **Table 7.** Corrected ocean pressure values starting at the indicated date and time for each station.
495 The duration of each survey is also provided. These values are also reflected in the plotted
496 offsets shown in Figure 5. Uncertainties listed are the quadrature sum of the total PGC error and
497 the RMS noise of the calibration pressure data.
498

Date	Time (UTC)	Duration	Pressure, no tidal correction (kPa)
O1			
2014-10-01	22:43:55	1h50m	29,588.15 ± 0.8
2014-10-02	06:15:30	1h51m	29,573.12 ± 0.8
2014-10-03	21:25:30	6h03m	29,578.76 ± 0.8
2015-10-21	05:05:30	2h03m	29,576.71 ± 0.8
2016-06-04	15:57:15	2h25m	29,574.90 ± 0.8
2017-09-06	10:58:00	1h58m	29,579.43 ± 0.8
O2			
2014-10-02	19:09:00	1h50m	19,418.44 ± 0.5
2014-10-03	01:21:05	1h56m	19,428.30 ± 0.5
2014-10-03	09:31:35	1h51m	19,408.89 ± 0.5
2015-10-20	23:56:00	1h50m	19,427.98 ± 0.5
2015-10-20	06:50:50	1h50m	19,409.00 ± 0.5
2016-06-05	21:44:45	1h46m	19,428.72 ± 0.5
2017-09-05	20:47:30	1h52m	19,428.11 ± 0.5
O2B			
2015-10-20	04:10:30	1h50m	19,420.10 ± 0.5
2016-06-05	19:11:35	2h22m	19,433.57 ± 0.5
O3			
2016-06-06	05:05:35	2h15m	13,397.88 ± 0.4
2017-09-05	05:46:50	2h08m	13,401.83 ± 0.4
O4			
2016-06-08	08:05:45	1h47m	6,388.54 ± 0.2
2017-09-04	17:35:50	2h06m	6,387.26 ± 0.2
O5			
2016-06-08	01:58:30	1h58m	885.41 ± 0.1
2017-09-02	23:50:30	2h29m	884.23 ± 0.1
2017-09-07	02:33:00	2h39m	880.51 ± 0.1
O6			
2016-06-07	18:30:50	2h11m	803.17 ± 0.1
2017-09-02	15:55:45	1h45m	812.32 ± 0.1
2017-09-07	12:27:30	1h36m	804.18 ± 0.1

499

Second, we also provide estimated secular deformation rates using surveys as individual points in long-term time series (Figure 7). Each point is the average of the absolute seafloor pressure with a tidal correction generated by SPOTL applied and a station specific offset removed for visual clarity (Agnew, 2012). We use tides generated by SPOTL in lieu of tides computed using harmonic analysis of continuous pressure data (e.g., t_tide) for consistency between all stations and years since continuous pressure data are not available for every occupation (Pawlowicz et al., 2012). Error bars and uncertainties represent the single standard deviation quadrature sum of errors attributed to the instrument measurements and RMS of the corrected, de-tided seafloor pressure. Most of the uncertainty at deeper stations is attributed to instrumental effects while the uncertainty at shallow stations is dominated by oceanographic processes whose effects will average out over long time spans of decades or more. The uncertainty of the estimated rates is inversely proportional to the total time span of the data and thus will improve with future measurements.

The surveys at each station suggest modest rates of motion equivalent to a few cm/year or less in most cases. These rates may be larger than the expected tectonic signals in the region, but they also likely contain oceanographic components due to aliasing that we cannot quantify presently. Nonetheless, the estimated rates are within a reasonable range given the uncertainties and generally agree with expected deformation patterns, i.e., subsidence near the trench (stations O1, O2) and uplift closer to the coast (stations O5, O6). Station O4 (Figure 7, bright yellow circle trace) is an exception, where the two surveys suggest a rate of +3.5 kPa/year is occurring (equivalent to 35 cm/year of height change), a rate that is nearly 4 times the estimated uncertainty and much larger than that observed elsewhere. We could not identify any egregious source of instrumental error, nor do we have a solution to mitigate this error at Station O4. The instrument and all components are handled meticulously and maintained, but we investigated potential sources of error of this magnitude (e.g., a mass change of 2 g, barometer calibrations, etc.). If it were attributed to components such as the piston-gauge area being chipped, damaged, or deformed, then that would produce similar discrepancies in the other stations and surveys. During the 2016 campaign at station O4, the ASCPR was moved from the ship freezer to the ship deck and prepared for loading on the ROV. The pressure case sphere was not fully sealed, so the instrument was returned to the ship freezer and resealed, which may have inadvertently caused a thermal shock to some component not captured by internal sensors. During the 2017 campaign, while recording at station O4, the ROV unexpectedly lost thruster control and came off bottom and moved the instrument from its placement on the benchmark. The ASCPR was quickly issued commands to stop the mass rotation and lock it in place as to not damage the PGC. We do not believe that the PGC was damaged, as this would be reflected in other measurements as well, but this event may have introduced some other unmodeled error when we resumed the measurement. The high rate may have been caused by aliasing of some very strong oceanographic signal. However, additional surveys spanning a greater time will eventually converge toward a more accurate value.

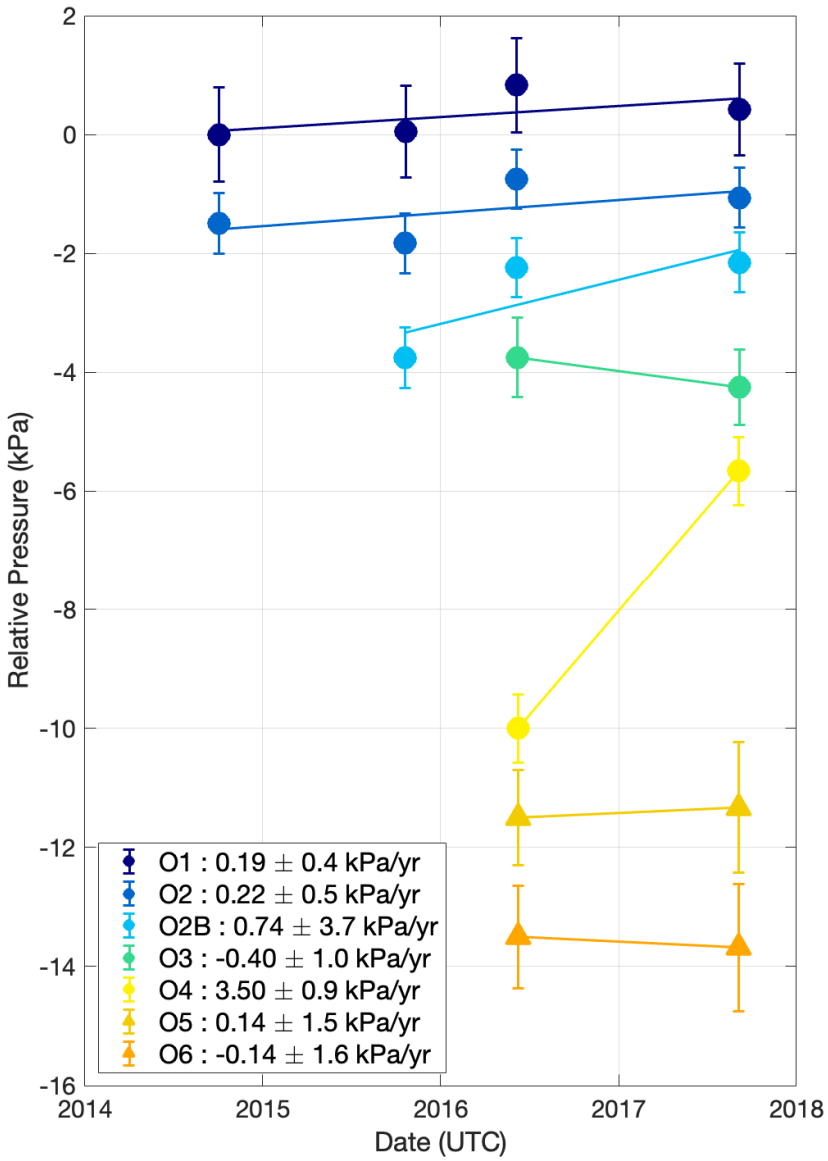

Figure 7. Pressure survey results from all stations. Estimated rates based on the individual surveys are listed. The plot shapes indicate the benchmark form factor (standard circular benchmark or triangular trawl-resistant benchmark). The inset legend provides the estimated pressure rates and uncertainties that were estimated by linear least squares fit. A pressure change of 0.1 kPa is equivalent to a height change of 1 cm.

Lastly, we leveraged our available continuous pressure data at station O1 to provide a better secular rate estimate. The ASCPR survey was treated as an individual calibration value used to calculate and remove only a long-term linear drift from the continuous record, which contains information on non-tidal oceanographic signals at periods shorter than the interval between surveys (8 to 12 months). Linear least squares fit to the difference between the overlapping absolute survey data and continuous BPR data was used to calculate the linear drift rate of the BPR, which was then removed from the continuous pressure record. The exponential component was not modeled because the small number of ASCPR surveys cannot sufficiently

constrain it, and the BPR was installed a few months prior to the first survey so the exponential component was likely less significant. The resulting drift-corrected pressure record was resampled to 30-minute intervals, de-tided using t_tide (Pawlowicz et al., 2012), and then lowpass filtered using a FIR filter with a passband at 1.2×10^{-6} Hz (0.10 cycles/day) and stopband at 7.7×10^{-6} Hz (0.067 cycles/day). A linear deformation rate was estimated from the record by linear least squares.

Station O1 had a single continuous BPR that spanned all the surveys conducted. This record was calibrated as described in section 2.5. The secular rate for station O1 based on continuous BPR data corrected for gauge drift using the absolute pressure surveys as calibration points is estimated and plotted in Figure 8. The continuous records at the other stations were insufficient for this analysis at this time, described in section 2.5. However, the BPRs deployed in 2017 were designed to record for 10 years, so additional absolute pressure surveys conducted before 2027 should allow those continuous data to be evaluated in this way.

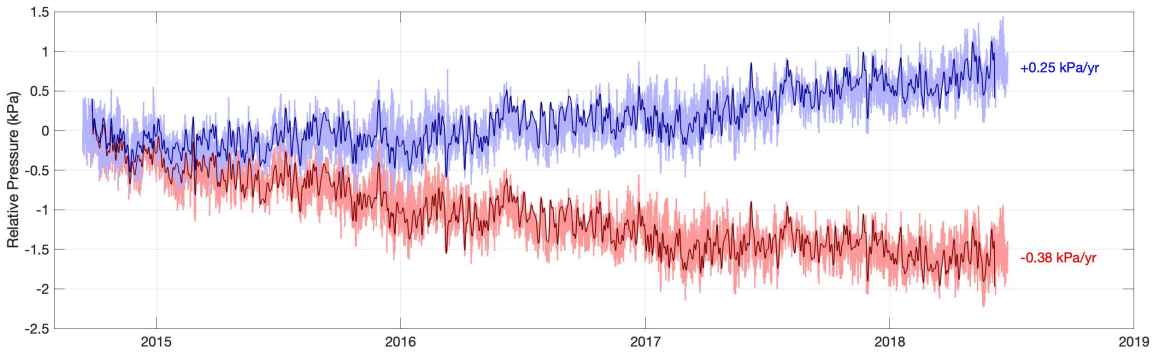

Figure 8. Continuous pressure record at station O1. The raw, uncalibrated pressure time series for is plotted in red. The pressure times series corrected for long-term, linear drift using absolute pressure surveys as calibration values is plotted in blue. The calibrated record reveals a significant difference and therefore drift, which could be mistakenly interpreted as a physical signal. Arbitrary offsets are plotted for clarity.

4 Conclusions

Absolute seafloor pressure surveys provide inherent value on their own as fiducial values. The ASCPR measurements can be used as longstanding benchmark values that can be incorporated into future geodetic studies. Each survey acts as a point in a long-term time series that could span decades or more and elucidate secular signals associated with tectonics or sea level rise. Additionally, the measurements' utility is improved if co-located with continuous BPR data, as they can be used to determine the long-term drift rate of the BPR and evaluated as a continuous record. Continuous pressure data also provide high-rate information useful for reducing aliasing and estimating long-period (daily to annual) oceanographic signals.

The disagreement between rates estimated using only individual surveys and rates from calibrated continuous data is attributed to aliased signals driven by physical oceanography. Most tidal analysis methods can typically remove up to 98% of the tidal signal, which still leaves several cm of uncertainty in each survey (Agnew, 2012; Pawlowicz et al., 2012). Additionally, any non-tidal effects from mesoscale eddies, currents, thermal fluctuations, or other causes are not addressed, which also contributes several cm of uncertainty in each survey. Advancements in satellite altimetry products, global and regional ocean models and hindcasts, CTD data, and

nearby pressure sensor networks could improve our ability to characterize and account for oceanographic-driven noise (Frederickson et al., 2019; Wilcock et al., 2021). Still, over shorter time periods (e.g., a few years) or when expected deformation rates are small (e.g., cm/year), the preferred method includes the use of co-located BPRs. If significantly longer time periods (e.g., decades) are expected or if expected deformation rates are large (e.g., tens of cm/year), then single point absolute pressure surveys can suffice on their own. In both cases, the estimated rate uncertainties will improve as the span of time between the first and last measurement increases.

These results demonstrate the capability of absolute seafloor pressure measurements for seafloor geodesy. Establishing additional time series of absolute measurements would be valuable for investigating other tectonic and oceanographic processes, such as the non-steric component of global sea level rise. Our results do not yet allow us to clearly discern between different expected vertical deformation rates associated with different models or studies that incorporate additional geodetic data to produce stronger geophysical interpretations, but that is outside the scope of this paper. However, the results do establish baseline vertical geodetic measurements in Cascadia and that, when compared to similar absolute measurements spanning several decades in the future, will be able to constrain secular vertical deformation rates.

Acknowledgments

This work was funded by NSF grants OCE 1558477 and OCE 1558468 and by a private donation from Jerome Paros. We would like to thank, John Delaney, Deb Kelley, David Price, Joel White, Heinz Wuhrmann, and Michael Davis. We also thank the crews of the R/V Thomas G. Thompson, R/V Roger Revelle, and R/V Sikuliaq, as well as the teams for ROV Jason II and ROV ROPOS. The authors have no conflicts of interest for this publication.

Open Research -- <u>data are not available presently yet, but we are working on publishing the data through these outlet(s)</u>

Data are available from the Marine Geoscience Data System (MGDS) at https://www.marine-geo.org/index.php and from the UC San Diego Library Digital Collections at http://library.ucsd.edu/dc/object/XXXXXXX. The published data have been parsed from raw data files and simply converted into physical units using manufacturer and lab calibrations. The raw data and calibration data are not published because it would be impractical to parse through the substantial amounts of ancillary data and formatting. However, the raw data, calibration data, and other supporting data may still be requested from corresponding author, Matthew J. Cook, or from author Glenn S. Sasagawa.

References

Agnew, D. C. (2012). SPOTL: Some Programs for Ocean-Tide Loading, *SIO Technical Report*. UC San Diego: Scripps Institution of Oceanography. https://escholarship.org/uc/item/954322pg

Atwater, B. F. (1987). Evidence for great Holocene earthquakes along the outer coast of Washington State. *Nature*, 236(4804), 942–944, https://doi.org/10.1126/science.236.4804.942

Atwater, B. F., Musumi-Rokkaku, S., Satake, K., Tsuji, Y., Ueda, K., & Yamaguchi, D. K. (2005). The orphan tsunami of 1700—Japanese clues to a parent earthquake in North America, *2nd ed.: Seattle, University of Washington Press*, U.S. Geological Survey Professional Paper 1707, 135. https://doi.org/10.3133/pp1707

Bean, V. E. (1994). NIST pressure calibration service, *U. S. Department of Commerce, CODEN: NSPUE2*, U. S. Government Printing Office, Washington, D. C., USA, Nat. Inst. Stand. Technol. Spec. Publ., 250-39.

Chadwell, C. D. (2016). Initiation of GPS-Acoustics measurements on the continental slope of the Cascadia Subduction Zone, Abstract T31C-2907 presented at the 2016 AGU Fall Meeting, San Francisco, CA, 12-16 Dec.

Chadwick Jr, W. W., Nooner, S. L., Zumberge, M. A., Embley, R. W., & Fox, C. G. (2006). Vertical deformation monitoring at Axial Seamount since its 1998 eruption using deep-sea pressure sensors. *J. of Volc. and Geotherm. Res.,* 150(1-3), 313-327. https://doi.org/10.1016/j.jvolgeores.2005.07.006

Fredrickson, E. K., Wilcock, W. S. D., Schmidt, D. A., MacCready, P., Roland, E., Kurapov, A. L., Zumberge, M. A., & Sasagawa, G. S. (2019). Optimizing sensor configurations for the detection of slow-slip earthquakes in seafloor pressure records, using the Cascadia Subduction Zone as a case study. *J. of Geophys. Res.: Solid Earth*, 124(12), 13504-13531. https://doi.org/10.1029/2019JB018053

Götze, H. J. (2011). International gravity formula. Encyclopedia of Solid Earth Geophysics, 611-612. https://doi.org/10.1007/978-90-481-8702-7_102

Machida, Y., Nishida, S., Kimura, T., & Araki, E. (2020). Mobile pressure calibrator for the development of submarine geodetic monitoring systems. *Journal of Geophysical Research: Solid Earth*, 125, e2020JB020284. https://doi.org/10.1029/2020JB020284

Matsumoto, Y., Ishikawa, T., Fujita, M., Sato, M., Saito, H., Mochizuki, M., Yabuki, T., & Asada, A. (2008). Weak interplate coupling beneath the subduction zone off Fukushima, NE Japan, inferred from GPS/acoustic seafloor geodetic observation. *Earth, Planets and Space*, 60(6), e9-e12. https://doi.org/10.1186/BF03353114

National Research Council (2012). Sea-Level Rise for the Coasts of California, Oregon, and Washington: Past, Present, and Future. *Washington, DC: The National Academies Press*. https://doi.org/10.17226/13389

Nooner, S. L., & Chadwick, W. W. (2009). Volcanic inflation measured in the caldera of Axial Seamount: Implications for magma supply and future eruptions. *Geochem. Geophys. Geosyst.*, 10(2), Q02002. https://doi.org/10.1029/2008GC002315

Nooner, S. L., & Chadwick, W. W. (2016). Inflation-predictable behavior and co-eruption deformation at Axial Seamount. *Science*, 354(6318), 1399-1403. https://doi.org/10.1126/science.aah4666

Paredes, X., Fandiño, O., Pensado, A. S., Comuñas, M. J. P., & Fernández, J. (2012). Experimental density and viscosity measurements of di(2ethylhexyl) sebacate at high pressure. *The Journal of Chemical Thermodynamics*, 44(1), 38-43. https://doi.org/10.1016/j.jct.2011.07.005

Paros, J. M., & Kobayashi, T. (2015a). Mathematical models of quartz sensor stability. Available at: http://paroscientific.com/pdf/G8095_Mathematical_Models.pdf

Pawlowicz, R., Beardsley, B., & Lentz, S. (2002). Classical tidal harmonic analysis including error estimates in MATLAB using T_TIDE. *Comp. & Geosci.*, 28(8), 929-937. https://doi.org/10.1016/S0098-3004(02)00013-4

Polster, A., Fabian, M., & Villinger, H. (2009). Effective resolution and drift of Paroscientific pressure sensors derived from long-term seafloor measurements. *Geochem. Geophys. Geosyst.*, 10(8). https://doi.org/10.1029/2009GC002532

Sasagawa, G. S., Cook, M. J., & Zumberge, M. A. (2016). Drift-corrected seafloor pressure observations of vertical deformation at Axial Seamount 2013-2014. *Earth and Space Science*, 3(9), 381-385. https://doi.org/10.1002/2016EA000190

Sasagawa, G. S., & Zumberge, M. A. (2013). A self-calibrating pressure recorder for detecting seafloor height change. *IEEE Journal of Oceanic Engineering*, 38(3), 447-454. https://doi.org/10.1109/JOE.2012.2233312

Segawa, J., & Fujimoto, H. (1988). Observation of an ocean bottom station installed in the Sagami Bay and replacement of the acoustic transponder attached to it, *JAMSTECTR Deep Sea Research*, *256*, 251-257.

Spiess, F. N., Chadwell, C. D., Hildebrand, J. A., Young, L. E., Purcell Jr, G. H., & Dragert, H. (1998). Precise GPS/Acoustic positioning of seafloor reference points for tectonic studies. *Physics of the Earth and Planetary Interiors*, 108(2), 101-112. https://doi.org/10.1016/S0031-9201(98)00089-2

719 Stenvold, T., Eiken, O., Zumberge, M. A., Sasagawa, G. S., & Nooner, S. L. (2006). High-
720 precision relative depth and subsidence mapping from seafloor water pressure measurements.
721 *SPE Journal*, 11, 380-381. https://doi.org/10.2118/97752-PA
722
723 Walton, M. A. L., Staisch, L. M., Dura, T., Pearl, J. K., Sherrod, B., Gomberg, J., Engelhart, S.,
724 Trehu, A., Watt, J., Perkins, J., Witter, R. C., Bartlow, N., Goldfinger, C., Kelsey, H., Morey,
725 A. E., Sahakian, V. J., Tobin, H., Wang, K., Wells, R., & Wirth, E. (2021). Toward an
726 integrative geological and geophysical view of Cascadia Subduction Zone earthquakes. *Ann.*
727 *Rev. of Earth and Plan. Sci.*, 49(1), 367-398. https://doi.org/10.1146/annurev-earth-071620-
728 065605
729
730 Wang, K., & Trehu, A. M. (2016). Invited review paper: Some outstanding issues in the study of
731 great megathrust earthquakes—The Cascadia example. *J. of Geodynamics*, 98, 1-18.
732 https://doi.org/10.1016/j.jog.2016.03.010
733
734 Watts, D. R., & Kontoyiannis, H. (1990). Deep-ocean bottom pressure measurement: Drift
735 removal and performance. *J. Atmos. Oceanic Technol*, 7(2), 296-306.
736 https://doi.org/10.1175/1520-0426(1990)007%3C0296:DOBPMD%3E2.0.CO;2
737
738 Watts, D. R., Wei, M., Tracey, K. L., Donohue, K. A., & He, B. (2021). Seafloor geodetic
739 pressure measurements to detect shallow slow slip events: Methods to remove contributions
740 from ocean water. *J. of Geophys. Res.: Solid Earth*, 126, e2020JB020065.
741 https://doi.org/10.1029/2020JB020065
742
743 Wearn, R. B., & Larson, N. G. (1982). Measurements of the sensitivities and drift of Digiquartz
744 pressure sensors. *Deep Sea Res. Part A. Oceanographic Research Papers*, 29(1), 111-134.
745 https://doi.org/10.1016/0198-0149(82)90064-4
746
747
748 Wilcock W. S. D., Manalang, D. A., Fredrickson, E. K., Harrington, M. J., Cram, G., Tilley, J.,
749 Burnett, J., Martin, D., Kobayashi, T., & Paros, J. M. (2021). A thirty-month seafloor test of
750 the A-0-A method for calibrating pressure gauges. *Front. Earth Sci.,* 8, 600671.
751 https://doi.org/10.3389/feart.2020.600671
752